Collaborative Guidance of UAV-Transported Semi-Flexible Payloads in Environments with Obstacles*

Aditya Hegde and Debasish Ghose

***Abstract*— Collaborative load manipulation and transportation is an emerging application of multi-unmanned aerial vehicle (UAV) systems. We address a problem where a team of UAVs transport a semi-flexible payload in an environment with multiple obstacles. By considering a semi-flexible payload, we restrict its flexibility to allow for safe-shape manipulation, which helps to navigate between obstacles while avoiding inter-UAV and payload-obstacle collisions. Control barrier functions (CBFs) are used to construct the obstacle avoidance and shape constraints, which are applied along with actuator constraints to an optimization-based control problem. The analysis is supported with simulation results for a team of four UAVs manipulating a payload in the presence of obstacles and settling on a standoff circle about a target.**

I. INTRODUCTION

Collaborative tasks involving teams of unmanned aerial vehicles (UAVs) have attracted the attention of researchers. Recent advancements in sensing and communication technology have made many UAV-collaborative tasks implementable [1]. The tasks vary from agricultural mapping [2], disaster site monitoring and rescue [3], [4], to collaborative-simulataneous localization and mapping (SLAM) [5]. An application where UAVs physically interact with the environment is payload transportation.

Collective payload transportation by multiple UAVs for payloads heavier than the lifting capacity of a single UAV [6], is required in many applications, such as UAVs transporting cable-suspended payloads [7], [8] and flexible fabrics [9]. Rigidly connected payloads are addressed in [10], where a pair of UAVs transport a payload connected to them electromagnetically, using vision-based sensing. Payloads connected to UAVs through spherical couplings [11] allow for the UAVs to act as thrust generators for payload manipulation, while decoupling the UAV and payload dynamics. A centralized-control architecture is often preferred in these applications.

The existence of obstacles in the environment requires the UAVs to modify their path collectively, to avoid payload-obstacle collisions. A potential field-approach to avoiding obstacle collisions is discussed for a problem of slung-load transportation by a pair of UAVs in [12]. However, the potential field approach does not provide an intuitive control design for obstacle avoidance of multiple UAVs and for rigidly connected payloads.

* Accepted at the IEEE Conference on Decision and Control - 2021

The authors are with the Department of Aerospace Engineering, Indian Institute of Science, Bangalore, India. adityahegde@iisc.ac.in, dghose@iisc.ac.in

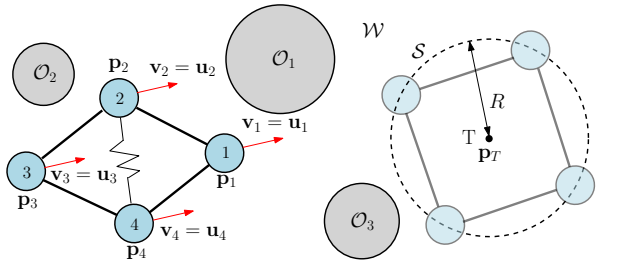

Fig. 1: Schematic diagram of 4 UAVs transporting a semi-flexible payload to a target T location with a standoff circle, while avoiding obstacles.

Motivated by the obstacle avoidance problem for rigidly-connected payloads, we present a control problem with 4 UAVs transporting a payload as they maneuver between obstacles and settle on a standoff circle about a target, while meeting shape and obstacle avoidance constraints designed using control barrier functions (CBFs). Such a problem formulation may be required for a team of UAVs surveying a target by collectively carrying a sensor suite mounted on booms connecting them. A few different configurations of payloads are presented in [13]. The work in this paper extends the two-UAV rigid payload transportation problem in [14], to an application with multiple UAVs and semi-flexible payloads requiring shape manipulation to navigate between obstacles. The idea of a semi-flexible payload comes from graph rigidity theory [15], with the payload being considered as a flexible graph, UAVs as the vertices, and sections of the payload between UAVs representing constant edge lengths (see Fig. 1). The payload is allowed to deform such that the distance between the unconnected vertices (UAVs) is regulated within specified bounds to restrict the flexibility of the graph. In contrast to problems with swarms of agents adjusting their mutual separation or splitting to navigate between obstacles, the problem presented here requires the UAVs to hold the formation and maintain mutual distances. An analogous representation of a spring between UAVs 2 and 4 is shown in Fig. 1, which can compress/expand when navigating between obstacles and return to its original length otherwise.

Control barrier functions have been applied to problems involving long duration autonomy of multi-robot systems [16], robotic-grasping [17], and adaptive-cruise control [18]. Their application to multi-robot systems with mutual collision avoidance is addressed in [19]. CBFs have also been used for obstacle avoidance of multiple robots [20], but not for obstacle avoidance of collaboratively transported objects. By using CBFs and an optimization-based controller in our

problem formulation, we

1) develop constraints for shape manipulation of the payload for obstacle avoidance.
2) bound the shape manipulation to ensure safety of the transporting UAVs, while maintaining edge lengths.
3) utilize the advantages of *local* navigation for obstacle avoidance, making it implementable on real-time platforms, using onboard sensors.

The paper is organized as follows - the problem description and preliminaries are covered in Section II. Section III discusses the construction of shape and obstacle avoidance constraints, first for a single obstacle, and then for a multi-obstacle problem. Simulation results with the proposed approach are presented in Section IV. Conclusions and future work are discussed in Section V.

II. Problem Description and Preliminaries

In this section, we describe the problem and system model, discuss the notations and results on CBFs used in the paper.

A. Notations and Operators

The set of real numbers is represented by $\mathbb{R}$. We represent vectors in lowercase bold and matrices in uppercase bold letters. We represent the identity matrix of size n by $\boldsymbol{I}_n$. The interior and boundary of a set $\mathcal{P}$ are represented by $\text{Int}(\mathcal{P})$ and $\partial\mathcal{P}$, respectively. The convex hull of $\mathcal{P}$ is represented by $\text{conv}(\mathcal{P})$. The Cartesian product of a set $\mathcal{P}$ with itself $\mathcal{P}\times\ldots\times\mathcal{P}$ (n-times) is denoted by $\mathcal{P}^n$. We define a circle $\mathcal{S}$ as a set of all points in a plane equidistant from a given point (center). The Euclidean-norm of a vector $\boldsymbol{x}\in\mathbb{R}^n$ is represented by $\|\boldsymbol{x}\|$, its infinity-norm by $\|\boldsymbol{x}\|_\infty \coloneqq \max\{|x_1|,|x_2|,\ldots,|x_n|\}$ and the unit vector along its direction is $\hat{\boldsymbol{x}}\in\mathbb{R}^n$. The inner product of two vectors $\boldsymbol{x},\boldsymbol{y}\in\mathbb{R}^n$ is $\langle\boldsymbol{x},\boldsymbol{y}\rangle$.

A graph is a pair $\mathcal{G}=(\mathcal{V},\mathcal{E})$, consisting of a finite set of vertices $\mathcal{V}$ and edges $\mathcal{E}\subseteq\mathcal{V}\times\mathcal{V}$. An edge $(j,k)\in\mathcal{E}$ consists of two nodes, indicating $j\in\mathcal{V}$ as the head and $k\in\mathcal{V}$ as the tail. An undirected edge is an unordered pair (j,k) representing mutual interaction. The graph $\mathcal{G}$ is called undirected if it consists of only undirected edges.

B. Problem Description and System Model

We assume a team of 4 UAVs transporting a continuous and flexible payload (see Fig. 1) represented by an undirected ring-topology graph $\mathcal{G}$, with UAVs as vertices in $\mathcal{V}=\{1,2,3,4\}$ and edges $\mathcal{E}=\{(1,2),(2,3),(3,4),(4,1)\}$. We assume the payload to be rigidly connected to the UAVs using spherical couplings [11], and the payload dynamics to be decoupled from the UAV dynamics. We also assume that the shape of the payload can change (within bounds) such that the edge lengths remain constant. The UAVs (and payload) execute planar motion in a space $\mathcal{W}\subseteq\mathbb{R}^2$ with obstacles that can be enclosed in balls $\mathcal{O}_m\subset\mathcal{W}$, such that the obstacles lie in $\text{Int}(\mathcal{O}_m)$ for all $m\in\{1,\ldots,M\}$. They are thus required to move and deform in the space $\mathcal{W}'\coloneqq\mathcal{W}\setminus\mathcal{O}$, where $\mathcal{O}=\cup_{i=1}^{M}\text{Int}(\mathcal{O}_m)$.

Assumption 1: We assume the payload to be mass-less for convenience in the analysis, and a physical realization of such a system will have compensatory control for inertial and contact forces.

The UAVs transport the payload as they finally settle on a standoff circle $\mathcal{S}$ about a stationary target T that is to be surveyed (see Fig. 1). In our problem, we consider multi-rotor UAVs controlled by an autopilot using velocity-based PD control [21]. Such UAVs can be represented by the following holonomic first-order system,

$$\dot{\boldsymbol{p}}_k=\boldsymbol{u}_k,\ \forall\ k\in\mathcal{V}, \tag{1}$$

where $\boldsymbol{p}_k\in\mathcal{W}'$ and $\boldsymbol{u}_k$ are the position and control input (and velocity reference for the autopilot) to the k^{th} UAV, respectively. Further, we account for actuator saturation by considering the following constraint,

$$\|\boldsymbol{u}_k\|_\infty\leq u_{\max},\ \forall\ k\in\mathcal{V}, \tag{2}$$

where, $u_{\max}>0$ bounds the components of control input.

C. Control Barrier Functions

Control barrier functions (CBFs) provide constraints in optimization-based control problems by identifying a safe set of operation for the system and using the system model to derive conditions for the forward invariance of this set. Thus, the control associated with a primary objective may be modified to ensure safe system operation. We use a problem formulation integrating the control Lyapunov function (CLF) with CBFs (CLF-CBF formulation) and the definition of a (reciprocal) barrier function [22], [16].

Definition 1 (Barrier function [22]): Consider a dynamical system $\dot{\boldsymbol{x}}=f(\boldsymbol{x})$ and a set $\mathcal{C}$ defined as $\mathcal{C}=\{\boldsymbol{x}\in\mathbb{R}^n\mid h(\boldsymbol{x})\geq 0\}$, with $\partial\mathcal{C}=\{\boldsymbol{x}\in\mathbb{R}^n\mid h(\boldsymbol{x})=0\}$, and $\text{Int}(\mathcal{C})=\{\boldsymbol{x}\in\mathbb{R}^n\mid h(\boldsymbol{x})>0\}$ for a smooth function $h:\mathbb{R}^n\to\mathbb{R}$. For this dynamical system, a function $B:\mathcal{C}\subset\mathbb{R}^n\to\mathbb{R}$ is a (reciprocal [16]) barrier function for the set $\mathcal{C}$ if there exist locally Lipschitz class $\mathcal{K}$ functions $\alpha_1,\alpha_2,\alpha_3$ such that, for all $\boldsymbol{x}\in\text{Int}(\mathcal{C})$, $\frac{1}{\alpha_1(h(\boldsymbol{x}))}\leq B(\boldsymbol{x})\leq\frac{1}{\alpha_2(h(\boldsymbol{x}))}$ and $\dot{B}(\boldsymbol{x})\leq\alpha_3(h(\boldsymbol{x}))$.

The following theorem, which utilizes Definition 1, will be useful for the analysis in subsequent sections.

Theorem 1 (Forward invariance of $\mathcal{C}$ [22]): Given a set $\mathcal{C}\subset\mathbb{R}^n$, if there exists a barrier function $B:\mathcal{C}\to\mathbb{R}$ as in Definition 1, then $\mathcal{C}$ is forward invariant.

In the following section, we identify the safe set for our problem and present an optimization-based controller which deforms the payload to prevent obstacle collisions.

III. Collision Avoidance Shape-Control

The main objective of the problem is the guidance of UAVs to a standoff circle about the target while controlling the inter-UAV distances. Further, the problem requires ii) payload-obstacle collision avoidance, and iii) bounded control inputs to the UAVs. The objectives are encoded as CLF-CBF constraints in a QP problem, which are active when the payload shape is close to its manipulation bounds or when the payload is close to obstacles. An additional constraint is placed to bound the control inputs.

We first propose the following unconstrained centralized-control QP problem,

$$\bar{\boldsymbol{u}} = \underset{\bar{\boldsymbol{u}}\in\mathbb{R}^8}{\operatorname{argmin}} \ \frac{1}{2}\ \bar{\boldsymbol{u}}^T \boldsymbol{Q}\bar{\boldsymbol{u}}, \tag{3}$$

where $\boldsymbol{Q}$ is a positive definite matrix and $\bar{\boldsymbol{u}} = [\boldsymbol{u}_1^T, \ldots, \boldsymbol{u}_4^T]^T \in \mathbb{R}^8$. The QP-problem is solved for all $t \geq 0$ along the trajectory of system (1) to achieve collective motion of the UAVs. We drop the representation for time-dependence of variables in (3) for brevity. Next, we sequentially discuss the constraints to be applied to the above formulation.

A. Bounded Shape-Control and Target Tracking

We perform this analysis in the obstacle-free space $\mathcal{W}$ and assume that the payload is flexible to allow shape change, but rigid in terms of restricting relative motion of the UAVs along the edges in $\mathcal{E}$. A deformation in the edge lengths will induce contact forces due to elasticity which in turn will affect UAV motion and stability. This requirement gives us the constraints on the relative velocity of UAVs along the edges. Let the distance between UAVs i and j for $(i,j) \in \mathcal{E}$, at time $t \geq 0$ be $\|\boldsymbol{p}_{i,j}(t)\| = \|\boldsymbol{p}_i(t) - \boldsymbol{p}_j(t)\|$, where, $\boldsymbol{p}_i(t)$ and $\boldsymbol{p}_j(t)$ are the positions of the two UAVs. Further, let the initial distance between them be $\|\boldsymbol{p}_{i,j}(0)\| = d,\ \forall (i,j) \in \mathcal{E}$. The following constraint maintains the edge lengths for all $t \geq 0$.

Lemma 1: Consider $(i,j) \in \mathcal{E}$ and a section of the payload held rigidly between UAVs i and j. The edge length between UAVs i and j is maintained to $\|\boldsymbol{p}_{i,j}(0)\| = d$ for all $t \geq 0$ if and only if,

$$\langle \boldsymbol{u}_i(t) - \boldsymbol{u}_j(t)\ ,\ \hat{\boldsymbol{p}}_{i,j}(t) \rangle = 0,\ \forall\ t \geq 0. \tag{4}$$

The constraints in Lemma 1 allow for deformation of the system of UAVs while meeting the edge length requirement, but may lead to collision of adjacent sections of the payload (edges). To avoid this, we place a constraint on the diagonally opposite UAVs of the system.

Lemma 2: Consider the diagonally opposite UAVs 1 and 3, and the constraints in Lemma 1. Then, the collision of any two sections of the payload is avoided if,

$$\delta_{\min} \leq \|\boldsymbol{p}_1(t) - \boldsymbol{p}_3(t)\| = \|\boldsymbol{p}_{1,3}\| \leq \delta_{\max}, \tag{5}$$

where $0 < \delta_{\min} < \delta_{\max} < 2d$.

Assuming an initial convex configuration of UAVs in the system, Lemmas 1 and 2 ensure that the convexity is preserved. The values of $\delta_{\min}, \delta_{\max}$ are chosen depending on design requirements. To enforce condition (5) we identify the following function using Definition 1,

$$h_s = (\|\boldsymbol{p}_{1,3}\| - \delta_{\min})\,(\delta_{\max} - \|\boldsymbol{p}_{1,3}\|) \tag{6}$$

for the safe set, $\mathcal{C}_s = \{(\boldsymbol{p}_1, \boldsymbol{p}_2, \boldsymbol{p}_3, \boldsymbol{p}_4) \in \mathcal{W}^4 \mid h_d = 0;\ h_s \geq 0\}$, where $h_d = 0$ represents the set of conditions $\|\boldsymbol{p}_{i,j}\| - d = 0,\ \forall (i,j) \in \mathcal{E}$. An associated barrier function is also proposed, $B_s = \frac{1}{h_s}, \dot{B}_s \leq \eta h_s$, which gives a constraint on the control inputs to UAVs 1 and 3,

$$-\langle \boldsymbol{u}_1 - \boldsymbol{u}_3\ ,\ \hat{\boldsymbol{p}}_{1,3} \rangle\,(\delta_{\min} + \delta_{\max} - 2\|\boldsymbol{p}_{1,3}\|) \leq \eta\,\delta, \tag{7}$$

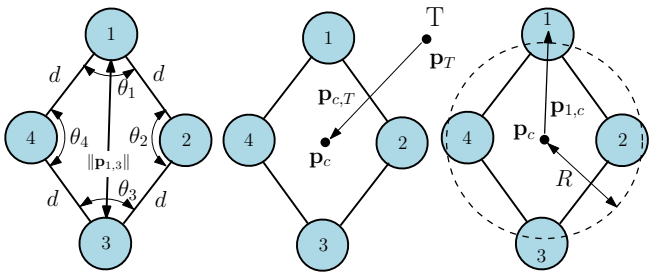

(a) Convex polygon (b) Target-tracking (c) Circle-tracking

Fig. 2: (a) Shape convexity preservation, $0 < \theta_k < \pi,\ \forall\ k \in \mathcal{V}$ if $0 < \|\boldsymbol{p}_{1,3}\| < 2d$; (b) Target standoff circle tracking of UAVs by driving centroid of the formation to the target and (c) driving UAV 1 to a circle of radius R about the centroid, in the absence of obstacles.

where, $\delta = \{(\|\boldsymbol{p}_{1,3}\| - \delta_{\min})(\delta_{\max} - \|\boldsymbol{p}_{1,3}\|)\}^3$, $\alpha_1(h_s) = \alpha_2(h_s) = h_s$, $\alpha_3(h_s) = \eta h_s$ (from Definition 1) and $\eta > 0$ is a constant.

Corollary 1: The UAVs form a convex polygon under Constraints (4) and (5) for all $t \geq 0$.

Proof: Assuming the initial configuration of UAVs to be convex (in the set $\mathcal{C}_s$), constraints (4) and (5) guarantee that the angles of the polygon $0 < \theta_k < \pi,\ \forall\ k \in \mathcal{V}$, the function $h_s \geq 0$, and the set $\mathcal{C}_s$ is forward invariant for all $t \geq 0$, using Definition 1 and Theorem 1 (see Fig. 2(a)). ■

The objective of guiding the UAVs to a standoff circle $\mathcal{S}$ is added to the formulation by designing two associated CLFs and enforcing the obtained constraints in the control optimization problem. Consider constraints (4) and (7), a stationary target and system (1) for this analysis. We propose a control law to guide the UAVs collectively to the standoff circle (see Figs. 2(b) and 2(c)) in the following theorem.

Theorem 2 (Standoff-circle convergence): The centroid of the system of UAVs (1) with positions $\boldsymbol{p}_k \in \mathcal{W}$, exponentially converges to the stationary target T position $\boldsymbol{p}_T \in \mathcal{W}$, if

$$\frac{1}{4}\left\langle \sum_{k=1}^{4} \boldsymbol{u}_k\ ,\ \boldsymbol{p}_{c,T} \right\rangle + \frac{\beta_T}{2}\,\|\boldsymbol{p}_{c,T}\|^2 \leq 0, \tag{8}$$

where, $\beta_T > 0$ is a constant, $\boldsymbol{p}_{c,T} = \boldsymbol{p}_c - \boldsymbol{p}_T$ and $\boldsymbol{p}_c = \sum_{k=1}^4 \boldsymbol{p}_k$ is the position of the centroid of the formation of UAVs. Further, the UAVs exponentially converge to the standoff circle $\mathcal{S}$ with radius R around the target if,

$$(\|\boldsymbol{p}_{1,c}\| - R)\,\langle \boldsymbol{u}_1 - \boldsymbol{u}_c\ ,\ \hat{\boldsymbol{p}}_{1,c} \rangle + \frac{\beta_c}{2}(\|\boldsymbol{p}_{1,c}\| - R)^2 \leq 0, \tag{9}$$

where, $\beta_c > 0$ is a constant, $\boldsymbol{p}_{1,c} = \boldsymbol{p}_1 - \boldsymbol{p}_c$ and $\boldsymbol{u}_c = \sum_{k=1}^4 \boldsymbol{u}_k$.

Proof: The objective of target-standoff circle tracking is achieved by simultaneously matching the centroid of the UAV formation with the target position, and controlling the distance of one of the UAVs from the centroid.

The first requirement is achieved by using the candidate Lyapunov function $U_1 = \frac{1}{2}\|\boldsymbol{p}_{c,T}\|^2$ and enforcing the inequality for exponential stability $\dot{U}_1 \leq -\beta_T U_1$, which gives inequality (8). The function U_1 is a valid Lyapunov function as it is radially unbounded, positive-definite and vanishes at $\boldsymbol{p}_{c,T} = 0$, which is one of the equilibrium conditions for standoff circle tracking.

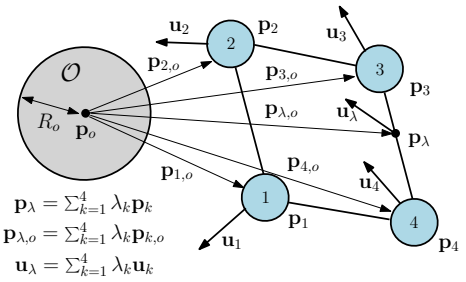

Fig. 3: Obstacle avoidance of a point $\boldsymbol{p}_{\boldsymbol{\lambda}}, \forall\, \boldsymbol{\lambda} \in \mathcal{L}$ on the payload.

We propose the candidate Lyapunov function $U_2 = \frac{1}{2}(\|\boldsymbol{p}_{1,c}\| - R)^2$ for controlling the distance of UAV 1 from the centroid of the formation, which translates to controlling the distance of the other UAVs from the centroid, under constraints (4) and (7). Like U_1, U_2 also satisfies the requirement of a Lyapunov function and vanishes at $\|\boldsymbol{p}_{1,c}\| = R$. Exponential convergence of the centroid-UAV 1 distance is guaranteed by enforcing the inequality $\dot{U}_2 \leq -\beta_c U_2$, which gives inequality (9). ■

B. Obstacle Avoidance: Single Obstacle

We first consider a single stationary obstacle in the space $\mathcal{W}$ and later extend our analysis to multiple obstacles. Let the obstacle be enclosed in a ball $\mathcal{O}_1 \subset \mathcal{W}$. Consider Constraints (4),(7) ensuring the convexity of the formation of UAVs, and the set $\mathcal{P} = \{\boldsymbol{p}_1, \boldsymbol{p}_2, \boldsymbol{p}_3, \boldsymbol{p}_4\}$. A point in conv$(\mathcal{P})$ has position $\boldsymbol{p}_{\boldsymbol{\lambda}} = \sum_{k=1}^4 \lambda_k \boldsymbol{p}_k$ for $\boldsymbol{\lambda} \in \mathcal{L} = \{\boldsymbol{\lambda} \mid \lambda_k \geq 0,\ \forall\, k \in \mathcal{V},\ \sum_{k=1}^4 \lambda_k = 1\}$. The payload forms the boundary of conv$(\mathcal{P})$, and thus a point on it, gives a sparse vector $\boldsymbol{\lambda}$. The dynamics of this point are $\dot{\boldsymbol{p}}_{\boldsymbol{\lambda}} = \boldsymbol{u}_{\boldsymbol{\lambda}} = \sum_{k=1}^4 \lambda_k \boldsymbol{u}_k$, where, $\boldsymbol{u}_{\boldsymbol{\lambda}}$ is the control input at the point (as seen in Fig. 3). Let the initial position of this point be in the safe set $\mathcal{W}' \equiv \mathcal{W} \setminus \text{Int}(\mathcal{O}_1)$. We construct a function $h_{\boldsymbol{\lambda}}$ and its associated barrier function $B_{\boldsymbol{\lambda}}$ for the safe set $\mathcal{W}'$ and the point $\boldsymbol{p}_{\boldsymbol{\lambda}}$, using Definition 1. Let R_o and $\boldsymbol{p}_o$ be the radius and center of the ball $\mathcal{O}_1$, respectively. Consider the function

$$h_{\boldsymbol{\lambda}} = \|\boldsymbol{p}_{\boldsymbol{\lambda},o}\| - R_o, \tag{10}$$

where $\boldsymbol{p}_{\boldsymbol{\lambda},o} = \boldsymbol{p}_{\boldsymbol{\lambda}} - \boldsymbol{p}_o$. The function $h_{\boldsymbol{\lambda}}$ is non-negative and smooth for all $\boldsymbol{p}_{\boldsymbol{\lambda}} \in \mathcal{W}'$ (for a fixed $\boldsymbol{\lambda}$), and with $h_{\boldsymbol{\lambda}} = 0$ for $\boldsymbol{p}_{\boldsymbol{\lambda}} \in \partial\mathcal{W}'$. We propose the following barrier function,

$$B_{\boldsymbol{\lambda}} = \frac{1}{h_{\boldsymbol{\lambda}}} = \frac{1}{\|\boldsymbol{p}_{\boldsymbol{\lambda},o}\| - R_o},\ \dot{B}_{\boldsymbol{\lambda}} \leq \gamma h_{\boldsymbol{\lambda}} = \gamma\,(\|\boldsymbol{p}_{\boldsymbol{\lambda},o}\| - R_o), \tag{11}$$

with $\alpha_1(h_{\boldsymbol{\lambda}}) = \alpha_2(h_{\boldsymbol{\lambda}}) = h_{\boldsymbol{\lambda}}$ and $\alpha_3(h_{\boldsymbol{\lambda}}) = \gamma h_{\boldsymbol{\lambda}}$ (from Definition 1), where, $\gamma > 0$ is a constant. Using (11), we get,

$$-\langle \boldsymbol{u}_{\boldsymbol{\lambda}}, \boldsymbol{p}_{\boldsymbol{\lambda},o} \rangle \leq \gamma \|\boldsymbol{p}_{\boldsymbol{\lambda},o}\| (\|\boldsymbol{p}_{\boldsymbol{\lambda},o}\| - R_o)^3, \tag{12}$$

a constraint on the control $\boldsymbol{u}_{\boldsymbol{\lambda}}$, which ensures that the set $\mathcal{W}'$ is forward invariant with respect to $\boldsymbol{p}_{\boldsymbol{\lambda}}$.

We now extend the above analysis to the system (1) and entire payload, $\boldsymbol{p}_{\boldsymbol{\lambda}}$ for all $\boldsymbol{\lambda} \in \mathcal{L}$. Further, we extend the definition of the safe set for the entire payload (and the UAVs) from $\mathcal{C}_s$ to $\mathcal{C}_{s,\boldsymbol{\lambda}} = \{(\boldsymbol{p}_1, \ldots, \boldsymbol{p}_4) \in \mathcal{W}'^4 \mid h_d = 0,\ h_s \geq 0, \text{conv}(\mathcal{P}) \subset \mathcal{W}'\}$, to account for the obstacle avoidance requirement. Using the definition of $h_{\boldsymbol{\lambda}}$ (10),

$$\mathcal{C}_{s,\boldsymbol{\lambda}} = \{(\boldsymbol{p}_1, \ldots, \boldsymbol{p}_4) \in \mathcal{W}'^4 \mid h_d = 0, h_s \geq 0, h_{\boldsymbol{\lambda}} \geq 0,\ \forall \boldsymbol{\lambda} \in \mathcal{L}\}. \tag{13}$$

The boundary of the safe set $\mathcal{C}_{s,\boldsymbol{\lambda}}$ is defined by the condition $h_s h_{\boldsymbol{\lambda}} = 0, \boldsymbol{\lambda} \in \mathcal{L}$. We note that the safe set formulation $\mathcal{C}_{s,\boldsymbol{\lambda}}$ includes infinite conditions $h_{\boldsymbol{\lambda}} \geq 0,\ \forall\ \boldsymbol{\lambda} \in \mathcal{L}$, corresponding to the obstacle avoidance of each point in conv$(\mathcal{P})$ and which translate to infinite constraints (12). Thus, we propose the following safe set, $\mathcal{C}_{s,\boldsymbol{\lambda}^\star}$ to handle the problem of infinite conditions.

Definition 2: The safe-set $\mathcal{C}_{s,\boldsymbol{\lambda}^\star}$ for system (1), under constraints (4) and (7), is

$$\begin{aligned}
\mathcal{C}_{s,\boldsymbol{\lambda}^\star} &= \{(\boldsymbol{p}_1, \ldots, \boldsymbol{p}_4) \in \mathcal{W}'^4 \mid h_d = 0,\ h_s \geq 0,\ h_{\boldsymbol{\lambda}^\star} \geq 0\} \\
\partial\mathcal{C}_{s,\boldsymbol{\lambda}^\star} &= \{(\boldsymbol{p}_1, \ldots, \boldsymbol{p}_4) \in \mathcal{W}'^4 \mid h_d = 0,\ h_s h_{\boldsymbol{\lambda}^\star} = 0\} \\
\text{Int}(\mathcal{C}_{s,\boldsymbol{\lambda}^\star}) &= \{(\boldsymbol{p}_1, \ldots, \boldsymbol{p}_4) \in \mathcal{W}'^4 \mid h_d = 0,\ h_s > 0,\ h_{\boldsymbol{\lambda}^\star} > 0\},
\end{aligned} \tag{14}$$

where $h_{\boldsymbol{\lambda}^\star} = \min_{\boldsymbol{\lambda} \in \mathcal{L}} h_{\boldsymbol{\lambda}}$, and $h_{\boldsymbol{\lambda}}$ is non-negative and smooth for $\boldsymbol{p}_{\boldsymbol{\lambda}} \in \mathcal{W}', \forall\ \boldsymbol{\lambda} \in \mathcal{L}$.

Lemma 3: The function $h_{\boldsymbol{\lambda}}, \boldsymbol{\lambda} \in \mathcal{L}$ is bounded below by $h_{\boldsymbol{\lambda}^\star} = \|\boldsymbol{p}_{\boldsymbol{\lambda}^\star,o}\| - R_o$, where $\boldsymbol{\lambda}^\star = \text{argmin}_{\boldsymbol{\lambda} \in \mathcal{L}} \|\boldsymbol{p}_{\boldsymbol{\lambda},o}\| - R_o$, and $\boldsymbol{p}_{\boldsymbol{\lambda}^\star} = \sum_{k=1}^4 \lambda_k^\star \boldsymbol{p}_k$.

Proof: The optimization problem $\min_{\boldsymbol{\lambda}}\ h_{\boldsymbol{\lambda}}$, with $\boldsymbol{\lambda} \in \mathcal{L}$, gives $\boldsymbol{\lambda}^\star$ as the solution. The point corresponding to $\boldsymbol{\lambda}^\star$, is $\boldsymbol{p}_{\boldsymbol{\lambda}^\star}$, which is the point on the payload closest to the ball $\mathcal{O}_1$ (and on the boundary of conv$(\mathcal{P})$) and gives the lower bound $h_{\boldsymbol{\lambda}^\star}$ on the function $h_{\boldsymbol{\lambda}}, \boldsymbol{\lambda} \in \mathcal{L}$. ■

We now propose the following result on the forward invariance of the set $\mathcal{C}_{s,\boldsymbol{\lambda}^\star}$.

Theorem 3: The set $\mathcal{C}_{s,\boldsymbol{\lambda}^\star}$ is forward invariant under the barrier functions

$$B_s = \frac{1}{h_s},\quad \dot{B}_s \leq \eta h_s, \tag{15}$$

$$B_{\boldsymbol{\lambda}^\star} = \frac{1}{h_{\boldsymbol{\lambda}^\star}},\ \dot{B}_{\boldsymbol{\lambda}^\star} \leq \gamma\ h_{\boldsymbol{\lambda}^\star}. \tag{16}$$

Proof: Using the definition of the safe set $\mathcal{C}_{s,\boldsymbol{\lambda}^\star}$ (14) and barrier function B_s (from the definition of $\mathcal{C}_s$), we get (15). Further, using Lemma 3 we have $h_{\boldsymbol{\lambda}^\star} = \|\boldsymbol{p}_{\boldsymbol{\lambda}^\star,o}\| - R_o$. Using Definitions 1 and 2, we construct $B_{\boldsymbol{\lambda}^\star}$ (16) with $\alpha_1(h_{\boldsymbol{\lambda}^\star}) = \alpha_2(h_{\boldsymbol{\lambda}^\star}) = h_{\boldsymbol{\lambda}^\star}$ and $\alpha_3(h_{\boldsymbol{\lambda}^\star}) = \gamma h_{\boldsymbol{\lambda}^\star}$, for the set $\mathcal{C}_{s,\boldsymbol{\lambda}^\star}$ (14). The rest of the proof follows as in [22]. ■

By using the analysis in Theorem 3, we reduce the collision avoidance problem to a single constraint associated with the point on the payload closest to the obstacle. The constraint obtained using the barrier function (16) is,

$$-\langle \boldsymbol{u}_{\boldsymbol{\lambda}^\star}, \boldsymbol{p}_{\boldsymbol{\lambda}^\star,o} \rangle \leq \gamma \|\boldsymbol{p}_{\boldsymbol{\lambda}^\star,o}\| (\|\boldsymbol{p}_{\boldsymbol{\lambda}^\star,o}\| - R_o)^3, \tag{17}$$

where, $\boldsymbol{u}_{\boldsymbol{\lambda}^\star} = \sum_{k=1}^4 \lambda_k^\star \boldsymbol{u}_k$ and $\boldsymbol{p}_{\boldsymbol{\lambda}^\star,o} = \boldsymbol{p}_{\boldsymbol{\lambda}^\star} - \boldsymbol{p}_o = \sum_{k=1}^4 \lambda_k^\star \boldsymbol{p}_{k,o}$. The positions of the UAVs relative to $\boldsymbol{p}_o$ are $\boldsymbol{p}_{k,o}$ for $k \in \mathcal{V}$.

C. Extension to Multiple Obstacles

We extend the above analysis to the case of multiple obstacles enclosed in balls $\mathcal{O}_m,\ m \in \{1, \ldots, M\}$ and define a $\boldsymbol{\lambda}_m^\star$−point below to help with the subsequent analysis.

Definition 3 ($\boldsymbol{\lambda}^\star_m-$point): A $\boldsymbol{\lambda}^\star_m-$point is the point on the payload closest to the ball $\mathcal{O}_m,\ m \in \{1,\dots,M\}$ such that $\boldsymbol{\lambda}^\star_m = \text{argmin}_{\boldsymbol{\lambda}_m \in \mathcal{L}} \|\boldsymbol{p}_{\boldsymbol{\lambda}_m,o_m}\| - R_{o_m}$. Here, $\boldsymbol{p}_{\boldsymbol{\lambda}_m,o_m} = \boldsymbol{p}_{\boldsymbol{\lambda}_m} - \boldsymbol{p}_{o_m} = \sum_{k=1}^4 \lambda_{k,m}\boldsymbol{p}_{k,o_m}$, $\lambda_{k,m}$ is the k^{th} component of $\boldsymbol{\lambda}_m$, R_{o_m} and $\boldsymbol{p}_{o_m}$ are the radius and center of the ball $\mathcal{O}_m$, respectively.

It is possible for the payload to be simultaneously close to multiple obstacles. Therefore, we redefine the safe set (14) and include simultaneous conditions $h_{\boldsymbol{\lambda}^\star_m} \geq 0$ for each obstacle (ball) $\mathcal{O}_m,\ m \in \{1,\dots,M\}$. We also propose the associated barrier functions, $B_{\boldsymbol{\lambda}^\star_m} = {}^1\!/_{h_{\boldsymbol{\lambda}^\star_m}}$, $\dot{B}_{\boldsymbol{\lambda}^\star_m} \leq \gamma\, h_{\boldsymbol{\lambda}^\star_m},\ m \in \{1,\dots,M\}$, using (11). We get the following constraints,

$$-\langle \boldsymbol{u}_{\boldsymbol{\lambda}^\star_m}, \boldsymbol{p}_{\boldsymbol{\lambda}^\star_m,o_m}\rangle \leq \gamma \|\boldsymbol{p}_{\boldsymbol{\lambda}^\star_m,o_m}\|(\|\boldsymbol{p}_{\boldsymbol{\lambda}^\star_m,o_m}\| - R_{o_m})^3, \quad \forall\ m \in \{1,\dots,M\}, \tag{18}$$

where $\boldsymbol{p}_{\boldsymbol{\lambda}^\star_m}$ is the position of the $\boldsymbol{\lambda}^\star_m-$point on the payload, and $\boldsymbol{u}_{\boldsymbol{\lambda}^\star_m} = \sum_{k=1}^4 \lambda^\star_{k,m}\boldsymbol{u}_k$ is the effective control input to be applied to the $\boldsymbol{\lambda}^\star_m$-point.

D. Constrained Optimization Problem and its Feasibility

We include all the constraints identified in Sections III-A to III-C, and account for actuator saturation (2) as discussed in Section II, to propose the following QP problem,

$$\begin{aligned}
\bar{\boldsymbol{u}} = \underset{(\tilde{\boldsymbol{u}},\zeta_1,\zeta_2)\in\mathbb{R}^{10}}{\text{argmin}}\ & \frac{1}{2}\tilde{\boldsymbol{u}}^T Q\tilde{\boldsymbol{u}} + w_1\zeta_1^2 + w_2\zeta_2^2 \\
\text{s.t.}\quad & \langle \boldsymbol{u}_i - \boldsymbol{u}_j\ ,\ \hat{\boldsymbol{p}}_{i,j}\rangle = 0,\ (i,j)\in\mathcal{E}, \\
& -\langle \boldsymbol{u}_1 - \boldsymbol{u}_3\ ,\ \hat{\boldsymbol{p}}_{1,3}\rangle(\delta_{\min} + \delta_{\max} - 2\|\boldsymbol{p}_{1,3}\|) \leq \eta\,\delta, \\
& \left\langle \sum_{k=1}^4 \boldsymbol{u}_k\ ,\ \boldsymbol{p}_{c,T}\right\rangle + \beta_T\|\boldsymbol{p}_{c,T}\|^2 \leq \zeta_1, \\
& (\|\boldsymbol{p}_{1,c}\| - R)\langle \boldsymbol{u}_1 - \boldsymbol{u}_c\ ,\ \hat{\boldsymbol{p}}_{1,c}\rangle + \beta_c(\|\boldsymbol{p}_{1,c}\| - R)^2 \leq \zeta_2, \\
& -\langle \boldsymbol{u}_{\boldsymbol{\lambda}^\star_m}, \boldsymbol{p}_{\boldsymbol{\lambda}^\star_m,o_m}\rangle \leq \gamma\|\boldsymbol{p}_{\boldsymbol{\lambda}^\star_m,o_m}\|(\|\boldsymbol{p}_{\boldsymbol{\lambda}^\star_m,o_m}\| - R_{o_m})^3, \\
& \qquad \forall\ m \in \{1,2,\dots,M\}, \\
& -u_{\max} \leq u_k^x,\ u_k^y \leq u_{\max},\ \forall\ k \in \mathcal{V},
\end{aligned} \tag{19}$$

where u_k^x and u_k^y are components of the control input $\boldsymbol{u}_k$. The slack variables $\zeta_1, \zeta_2 \in \mathbb{R}$ are included in the CLF constraints for the solvability of the problem and prioritize safety over target tracking, while $w_1, w_2 > 0$ are their associated penalties in the objective function.

Theorem 4: The QP problem (19) is recursively feasible for system (1) for all $t \geq 0$.

Proof: The problem (19) is a QP formulation with a linear equality constraint (4) and affine inequality constraints. Further, since (1) is a first-order system and the control $\bar{\boldsymbol{u}}$ is a velocity, it can be chosen to satisfy the constraints in (19). Thus, beginning in the safe set $\mathcal{C}_{s,\boldsymbol{\lambda}^\star}$, Theorem 3 guarantees that $\bar{\boldsymbol{u}}$ (solution to (19)) keeps the system in the safe set. Consider the control $\boldsymbol{u}_k = \boldsymbol{u},\ \forall k \in \mathcal{V}$, which satisfies the edge constraints (4) and the CBF constraint (7) for system (1) being in the safe set ($\delta \geq 0$). The control $\boldsymbol{u}$ can be selected to satisfy the CBF constraint (18) and the actuator saturation bounds $u_{\max}$. One such control is $\boldsymbol{u} = [0,0]^T$ ($\|\boldsymbol{p}_{\boldsymbol{\lambda}^\star_m,o_m}\| - R_{o_m} \geq 0, \forall\ m \in \{1,\dots,M\}$ in the safe set). Under this control, the slack variables ζ_1 and ζ_2 can be chosen to satisfy the CLF constraints, as a solution of (19). Thus, the feasible set is non-empty for all $t \geq 0$, which guarantees the feasibility of (19) for all $t \geq 0$, and thus its recursive feasibility. ■

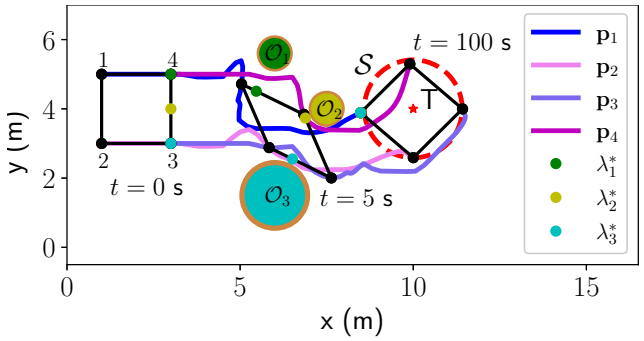

Fig. 4: Trajectories of the system of UAVs and payload in environment with obstacle-enclosing balls $\mathcal{O}_1, \mathcal{O}_2, \mathcal{O}_3$. UAVs settle on standoff circle $\mathcal{S}$ about a target T. Positions of the payload at time, $t = [0,\ 5,\ 100]$ s and the associated $\boldsymbol{\lambda}^\star_1, \boldsymbol{\lambda}^\star_2, \boldsymbol{\lambda}^\star_3$ points are also plotted. Link to animation: `https://github.com/aadih88/CollabUAV_paytrans`.

IV. Simulation Results

We present simulations for a team of 4 UAVs with initial positions $\boldsymbol{p}_1 = [1.0,\ 5.0]^T$ m, $\boldsymbol{p}_2 = [1.0,\ 3.0]^T$ m, $\boldsymbol{p}_3 = [3.0,\ 3.0]^T$ m and $\boldsymbol{p}_4 = [3.0,\ 5.0]^T$ m, such that they form a square with sides of length $\|\boldsymbol{p}_{i,j}\| = d = 2$ m, $\forall\ (i,j) \in \mathcal{E}$, which are to be held constant. The shape change is allowed to let the distances between the diagonally opposite UAVs, $\|\boldsymbol{p}_{1,3}\|$ and $\|\boldsymbol{p}_{2,4}\|$ to vary. The UAVs are required to settle on a standoff circle of radius $R = \sqrt{2}$ m around a stationary target T at $\boldsymbol{p}_T = [10.0,\ 4.0]^T$ m. We consider $M = 3$ obstacles and the balls enclosing them with center and radii, $\mathcal{O}_1$: $\boldsymbol{p}_{o_1} = [6.0,\ 5.6]^T$ m, $R_{o_1} = 0.5$ m; $\mathcal{O}_2$: $\boldsymbol{p}_{o_2} = [7.5,\ 4.0]^T$ m, $R_{o_2} = 0.5$ m; $\mathcal{O}_3$: $\boldsymbol{p}_{o_3} = [6.0,\ 1.5]^T$ m, $R_{o_3} = 1.0$ m. The parameters in the QP-problem (19) are as follows. The constant $\eta = 5$ constrains the inter-UAV distance $\|\boldsymbol{p}_{1,3}\|$ between $\delta_{\min} = 1$ m and $\delta_{\max} = 3.87$ m. It is to be noted that fixing either of $\delta_{\min}$, $\delta_{\max}$ defines the other as the payload length d between UAVs is constrained to be constant. The constants in the CLF constraints are $\beta_T = 2$ and $\beta_c = 2$. The slack variables ζ_1 and ζ_2 are penalized by the parameters $w_1 = 2$ and $w_2 = 4$. The matrix $\boldsymbol{Q} = \boldsymbol{I}_8$. The constant for the obstacle avoidance constraint is $\gamma = 10$. The bound on the control (2) is $u_{\max} = 1.0$ m/s.

The trajectories of the UAVs and payload, and the obstacle enclosing balls $\mathcal{O}_1, \mathcal{O}_2, \mathcal{O}_3$ are shown in Fig. 4. We also plot the positions of the payload and the $\boldsymbol{\lambda}^\star_1, \boldsymbol{\lambda}^\star_2, \boldsymbol{\lambda}^\star_3-$points at times, $t = [0,\ 5,\ 100]$ seconds. The $\boldsymbol{\lambda}^\star_m-$points change as the orientation and position of the system relative to the obstacles changes. The payload does not touch the balls as seen in Fig. 5(b), where the closest payload-obstacle distances are greater than zero ($h_{\boldsymbol{\lambda}^\star_m} > 0$ for $m = \{1,2,3\}$). The shape of the system changes relative to its initial square configuration, and the distances between diagonally opposite UAVs change within bounds (see Fig. 6(b)) as the payload maneuvers through the gap between the obstacles. The payload shape gradually changes back to its initial square configuration after moving past the obstacles at $t = 5$ s. This behavior is also seen in Figs. 5(a) and 5(b), where the UAV-target distances

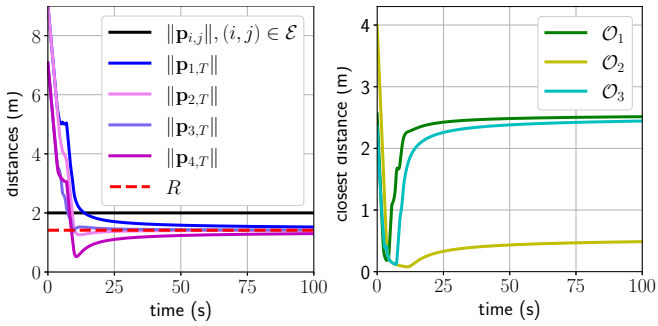

(a) UAV-target distances (b) Obstacle distances

Fig. 5: (a) UAV-target distances, and inter-UAV distances for the edge set $\mathcal{E}$, and (b) closest distance of payload to obstacles.

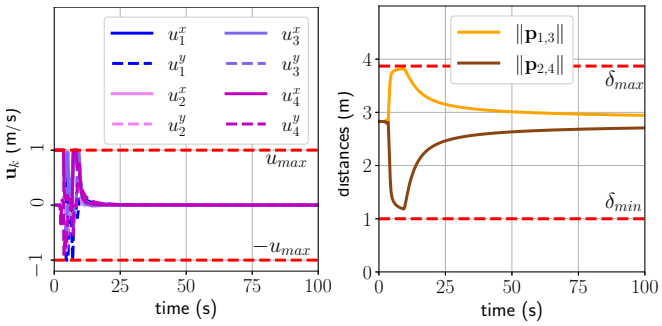

(a) Control inputs (b) Diagonal UAVs distance

Fig. 6: (a) Bounded control inputs (components) and (b) distances between diagonally opposite UAVs.

significantly reduce and obstacle distances are the least at this time. Standoff circle convergence is exponentially achieved as the UAVs continue to settle and the $\boldsymbol{\lambda}_m^\star-$points coincide at $t = 100$ s, located at UAV 1 ($\boldsymbol{p}_1$). The UAV-target distances are plotted in Fig. 5(a), showing convergence to the standoff circle. The inter-UAV distance is constant at $\|\boldsymbol{p}_{i,j}(t)\| = d = 2$ m, for all $t \geq 0$, $\forall\ (i,j) \in \mathcal{E}$, during the simulation.

The payload moves slowly after $t = 9$ s due to exponential convergence to the standoff circle, which is clear from the low values of control input $\boldsymbol{u}_k$, $\forall\ k \in \mathcal{V}$ in Fig. 6(a). The control bounds $u_{\max}$ (in Fig. 6(a)) are also satisfied.

V. CONCLUSIONS AND FUTURE WORK

In this paper, we presented a collaborative semi-flexible payload transportation and manipulation problem with a team of 4 UAVs. The collision amongst UAVs and sections of the payload were prevented by designing constraints using CBFs. The problem formulation assured collision avoidance of the UAVs and payload with obstacles, by identification of the safe set of operation and its associated CBF. The problem was formulated with a single constraint associated with the point on the payload closest to the obstacle, thus avoiding an infinite constraint problem. Simulation results were presented for a team of UAVs manipulating a payload to navigate between 3 obstacles and settle on a standoff circle. The obstacles were considered to be enclosed by balls and an extension to other convex enclosures will augment the results presented in this paper. There may exist several (undesirable) local equilibria of (1) in the presence of obstacles, depending on obstacle size and positions in space, initial positions of the UAVs, target location and standoff circle radius. The equilibrium conditions can be obtained using the Karush-Kuhn-Tucker conditions and an analysis of these conditions will be beneficial in finding algorithms to navigate the system away from the undesired equilibria and to the target location.

REFERENCES

[1] J. Gu, T. Su, Q. Wang, X. Du, and M. Guizani, "Multiple moving targets surveillance based on a cooperative network for multi-UAV," *IEEE Communications Magazine*, vol. 56, no. 4, pp. 82–89, 2018.

[2] D. Albani, D. Nardi, and V. Trianni, "Field coverage and weed mapping by UAV swarms," in *IEEE/RSJ International Conference on Intelligent Robots and Systems (IROS)*, 2017, pp. 4319–4325.

[3] A. Kanzaki and H. Akagi, "A UAV-collaborative sensing method for efficient monitoring of disaster sites," in *Advanced Information Networking and Applications*, L. Barolli, M. Takizawa, F. Xhafa, and T. Enokido, Eds. Cham: Springer International Publishing, 2020, pp. 775–786.

[4] E. T. Alotaibi, S. S. Alqefari, and A. Koubaa, "LSAR: Multi-UAV collaboration for search and rescue missions," *IEEE Access*, vol. 7, pp. 55 817–55 832, 2019.

[5] P. Schmuck and M. Chli, "Multi-UAV collaborative monocular SLAM," in *IEEE International Conference on Robotics and Automation (ICRA)*, 2017, pp. 3863–3870.

[6] D. K. D. Villa, A. S. Brandão, and M. Sarcinelli-Filho, "A survey on load transportation using multirotor UAVs," *Journal of Intelligent and Robotic Systems*, vol. 98, no. 2, pp. 267–296, 2020.

[7] X. Zhang, F. Zhang, P. Huang, J. Gao, H. Yu, C. Pei, and Y. Zhang, "Self-triggered based coordinate control with low communication for tethered multi-UAV collaborative transportation," *IEEE Robotics and Automation Letters*, vol. 6, no. 2, pp. 1559–1566, 2021.

[8] J. Geng and J. W. Langelaan, "Implementation and demonstration of coordinated transport of a slung load by a team of rotorcraft," in *AIAA Scitech Forum*, 2019, ch. 0913.

[9] R. Cotsakis, D. St-Onge, and G. Beltrame, "Decentralized collaborative transport of fabrics using micro-UAVs," in *International Conference on Robotics and Automation (ICRA)*, 2019, pp. 7734–7740.

[10] G. Loianno and V. Kumar, "Cooperative transportation using small quadrotors using monocular vision and inertial sensing," *IEEE Robotics and Automation Letters*, vol. 3, no. 2, pp. 680–687, 2018.

[11] H.-N. Nguyen, S. Park, and D. Lee, "Aerial tool operation system using quadrotors as rotating thrust generators," in *IEEE/RSJ International Conference on Intelligent Robots and Systems*, 2015, pp. 1285–1291.

[12] I. H. B. Pizetta, A. S. Brandão, and M. Sarcinelli-Filho, "Avoiding obstacles in cooperative load transportation," *ISA Transactions*, vol. 91, pp. 253–261, 2019.

[13] D. Mellinger, M. Shomin, N. Michael, and V. Kumar, *Cooperative Grasping and Transport Using Multiple Quadrotors*. Berlin, Heidelberg: Springer Berlin Heidelberg, 2013, pp. 545–558.

[14] A. Hegde and D. Ghose, "Multi-UAV collaborative transportation of payloads with obstacle avoidance," *IEEE Control Systems Letters*, vol. 6, pp. 926–931, 2022.

[15] S. Zhao and D. Zelazo, "Bearing rigidity theory and its applications for control and estimation of network systems: Life beyond distance rigidity," *IEEE Control Systems Magazine*, vol. 39, no. 2, pp. 66–83, 2019.

[16] A. D. Ames, S. Coogan, M. Egerstedt, G. Notomista, K. Sreenath, and P. Tabuada, "Control barrier functions: Theory and applications," in *18th European Control Conference (ECC)*, 2019, pp. 3420–3431.

[17] W. Shaw Cortez, D. Oetomo, C. Manzie, and P. Choong, "Control barrier functions for mechanical systems: Theory and application to robotic grasping," *IEEE Transactions on Control Systems Technology*, vol. 29, no. 2, pp. 530–545, 2021.

[18] W. Xiao and C. Belta, "Control barrier functions for systems with high relative degree," in *58th IEEE Conference on Decision and Control (CDC)*, 2019, pp. 474–479.

[19] L. Wang, A. D. Ames, and M. Egerstedt, "Safety barrier certificates for collisions-free multirobot systems," *IEEE Transactions on Robotics*, vol. 33, no. 3, pp. 661–674, 2017.

[20] Y. Chen, A. Singletary, and A. D. Ames, "Guaranteed obstacle avoidance for multi-robot operations with limited actuation: A control barrier function approach," *IEEE Control Systems Letters*, vol. 5, no. 1, pp. 127–132, 2021.

[21] "Multicopter control architecture," PX4 User Guide. [Online]. Available: https://docs.px4.io/master/en/flight_stack/controller_diagrams.html

[22] A. D. Ames, J. W. Grizzle, and P. Tabuada, "Control barrier function based quadratic programs with application to adaptive cruise control," in *53rd IEEE Conference on Decision and Control*, 2014, pp. 6271–6278.